THE JOURNAL OF BIOLOGICAL CHEMISTRY VOL. 285, NO. 9, pp. 6371–6376, February 26, 2010

Structure of GroEL in Complex with an Early Folding Intermediate of Alanine Glyoxylate Aminotransferase*[S]

Received for publication, September 4, 2009, and in revised form, January 7, 2010 Published, JBC Papers in Press, January 7, 2010, DOI 10.1074/jbc.M109.062471

Armando Albert[‡1], Cristina Yunta[§], Rocío Arranz[¶], Álvaro Peña[¶], Eduardo Salido[§], José María Valpuesta[¶], and Jaime Martín-Benito[¶]

From the [‡]Grupo de Cristalografía Macromolecular y Biología Estructural, Instituto de Química Física "Rocasolano," Consejo Superior de Investigaciones Científicas, Madrid E-28006, [§]Centro de Investigacíon Biomédica en Red de Enfermedades Raras, Hospital Universitario Canarias-Instituto de Tecnologias Biomédicas, University La Laguna, Tenerife E-38320, and [¶]Centro Nacional de Biotecnología, Consejo Superior de Investigaciones Científicas, Campus Universidad Autónoma de Madrid, Madrid E-28049, Spain

Primary hyperoxaluria type 1 is a rare autosomal recessive disease caused by mutations in the alanine glyoxylate aminotransferase gene (AGXT). We have previously shown that P11L and I340M polymorphisms together with I244T mutation (AGXT-LTM) represent a conformational disease that could be amenable to pharmacological intervention. Thus, the study of the folding mechanism of AGXT is crucial to understand the molecular basis of the disease. Here, we provide biochemical and structural data showing that AGXT-LTM is able to form non-native folding intermediates. The three-dimensional structure of a complex between the bacterial chaperonin GroEL and a folding intermediate of AGXT-LTM mutant has been solved by cryoelectron microscopy. The electron density map shows the protein substrate in a non-native extended conformation that crosses the GroEL central cavity. Addition of ATP to the complex induces conformational changes on the chaperonin and the internalization of the protein substrate into the folding cavity. The structure provides a three-dimensional picture of an *in vivo* early ATP-dependent step of the folding reaction cycle of the chaperonin and supports a GroEL functional model in which the chaperonin promotes folding of the AGXT-LTM mutant protein through forced unfolding mechanism.

Chaperonins are ATP-dependent molecular machines that are able to bind misfolded protein substrates and promote their proper folding (1). Protein misfolding is the main mechanism involved in a large number of genetic diseases caused by missense mutations, giving rise to the concept of "conformational diseases " (2, 3). The role of chaperones in the pathogenesis of conformational diseases has been recently reviewed (4). A deficiency of the hepatic enzyme alanine glyoxylate aminotransferase (AGXT,[2] also known as AGT) is responsible for the rare hereditary disease primary hyperoxaluria type 1 (PH1, Online Mendelian Inheritance in Man (OMIM) 259900). Insufficient AGXT activity leads to increased conversion of the substrate glyoxylate to the toxic ion oxalate, which subsequently accumulates as insoluble calcium salt in the kidney. In the later stages of the disease, calcium oxalate deposition becomes widespread and life-threatening unless liver and kidney transplantation is performed (5). Most of the PH1 alleles detected in the Canary Islands patients carry the I244T mutation together with the polymorphisms P11L and I340M. These amino acid changes result in a misfolded protein (AGXT-LTM) that undergoes stable interaction with molecular chaperones and aggregation (6). A large number of the pathogenic variants of this protein are the result of missense mutations that are likely to result in misfolded proteins (7). Thus, the study of these folding intermediates and the effect of the point mutations on the structure of the protein are central to elucidate the molecular basis responsible for the PH1 disease.

The bacterial chaperonin-cochaperonin GroEL-GroES system is well characterized both at the biochemical and structural level (8, 9). GroEL is a large homo-oligomeric barrel structure formed by two rings each one comprising 7 subunits of a 57-kDa polypeptide chain. Each GroEL ring displays a large central cavity lined by hydrophobic residues at its entrance, which are responsible for substrate binding (10). GroES is a 70-kDa homoheptameric ring that caps both ends of the GroEL barrel and plays an important role in the folding cycle of GroEL (11). The GroEL folding cycle first includes binding of a protein substrate to the apical domains of one of the rings (the cis-ring) followed by binding of ATP and GroES. This triggers a conformational change that makes the central cavity hydrophilic and leads to the encapsulation of the protein substrate. Binding of GroES and ATP to the opposite ring (trans-ring) results in the release of a properly folded protein substrate. The protein molecules that fail to fold are re-captured by GroEL for another reaction cycle. Single-molecule fluorescence resonance energy transfer experiments have been used to trap and follow the substrate conformational changes during the reaction cycle (12–15). First, it has been shown that ATP-mediated expansion of the GroEL apical domain induces the stretching of the partially folded protein substrates. This expansion actively facilities the folding by positioning a partially folded protein to a higher point in the energy landscape. Second, GroES binding

* This work was supported by Grants BFU2008-00368/BMC (to A. A.), BFU2007-62382/BMC (to J. M. V.), and SAF2007-62343 (to E. S.) from the Spanish "Plan Nacional" (Ministerio de Ciencia e Innovacíon) and "Factoría de Cristalización" Consolider Ingenio 2010 (to A. A.).

[S] The on-line version of this article (available at http://www.jbc.org) contains supplemental Figs. S1–S3.

[1] To whom correspondence should be addressed: Grupo de Cristalografía Macromolecular y Biología Estructural, Instituto de Química Física "Rocasolano," Consejo Superior de Investigaciones Científicas, Serrano 119, Madrid E-28006, Spain. Fax: 34915642431; E-mail: xalbert@iqfr.csic.es.

[2] The abbreviations used are: AGXT, alanine glyoxylate aminotransferase; PH1, primary hyperoxaluria type 1; Cryo-EM, cryoelectron microscopy.

produce a controlled collapse of the substrate during the release into the chaperonin cavity.

To investigate the AGXT-LTM conformational changes responsible for PH1 in our patients, we have used an *Escherichia coli* strain that overexpresses GroEL-GroES system and AGXT-LTM protein. This enables trapping of *in vivo* folding intermediates of mutant AGXT and GroEL. This complex was reconstructed three-dimensionally by cryoelectron microscopy (Cryo-EM) and image-processing techniques, providing information of an early stage in the folding reaction cycle. The electron density map reveals that AGXT-LTM crosses the GroEL central cavity, making contacts with the apical domains of distant GroEL subunits. An atomic model of AGXT derived from its x-ray structure (16) fits very well with the mass of the complex attributable to AGXT-LTM mutant protein, suggesting that the mutant protein is able to fold partially. Such folding intermediates could be targeted by molecular chaperones or other drugs to rescue the native conformation. Our results support the hypothesis that the assisted folding of AGXT-LTM mutant is driven through the forced unfolding of a quasi-native state of the protein.

EXPERIMENTAL PROCEDURES

Cell Culture and Transformations—Top10 *E. coli* (Invitrogen) were transformed with AGXT constructs (6) and GroEL-ES plasmids (Takara, Inc.), using standard protocols (17). They were grown at 37 °C in LB broth. GroEL-GroES expression was induced with 2 mg/ml L-arabinose at the beginning of the culture. AGXT expression was induced with 0.5 mM isopropyl-D-thiogalactoside when the A_{600} was 0.4–0.6, and the culture was incubated for an additional 4 h at 25 °C.

AGXT Enzymatic Assay—AGXT activity from the soluble extract was determined as described (6). Activity units are expressed as micromoles of pyruvate/h/mg of total protein.

Western Blotting—Cell pellets from 1 ml of culture were sonicated in 100 μl (50 mM Tris-HCl (pH 7.4), 150 mM NaCl, protease inhibitors (Complete; Roche Applied Science) 0.05% Nonidet P-40, and 0.05% Triton X-100). The soluble fraction was separated by centrifugation, and the protein concentration was measured with bicinchoninic acid. Equal amounts of each extract (1 μg) were analyzed by immunoblotting (17) with anti-hAGXT (1:5,000) (rabbit, raised against recombinant AGXT). Peroxidase-conjugated anti-rabbit IgG (Jackson ImmunoResearch) was used as secondary antibody (1:10,000), and the chemiluminescence substrate was from Pierce.

Protein Purification—Cells were harvested, and the His-tagged AGXT was purified using HisTrap FF columns (GE Healthcare) according to the manufacturer's instructions. Soluble AGXT was batch-purified under native conditions, and it was eluted from the Ni^{2+} resin in a buffer with 500 mM imidazole. Imidazole was removed using a PD-10 column (GE Healthcare), and protein was concentrated by filtration (Ultra-Free 0.5, Millipore Corporation). GroEL was copurified with AGXT due to protein-protein interactions. Purified proteins were subjected to a size-exclusion chromatography (Bio-Silect SEC 250; Bio-Rad) to isolate the complex. The purified complex was used to test the effect of ATP in the interaction between both proteins after 20 min of incubation.

Electron Microscopy—For electron microscopy of negatively stained samples, 5-μl aliquots of a solution containing 0.05 mg/ml GroEL·AGXT-LTM complexes buffered with 10 mM Tris-HCl (pH 7.5), 50 mM NaCl were applied to glow-discharged carbon-coated collodion grids for 1 min and then stained for 1 min with 2% uranyl acetate. Images were recorded in a JEOL 1200EX-II electron microscope operated at 100 kV and recorded at 20,000 nominal magnification. For Cryo-EM, 5-μl aliquots were applied to holey carbon grids (Quantifoil) for 2 min, blotted for 5 s, and frozen rapidly in liquid ethane. Images were recorded under minimum dose conditions in a FEI G2 FEG electron microscope operated at 200 kV using a Gatan cold stage and recorded on Kodak SO-163 film at 50,000 nominal magnification between 1.5 and 3.0 μm underfocus.

Image Processing, Two-dimensional Averaging, and Three-dimensional Reconstruction—Micrographs were digitized in a Zeiss Photoscan scanner with a final sampling window corresponding to 3.5 Å/pixel for negatively stained samples and 2.8 Å/pixel for vitrified samples. Contrast transfer function of micrographs was estimated using CTFFIND software (18) and corrected using BSOFT (19). Images were two-dimensionally processed and aligned using maximum likelihood reference-free methods with the XMIPP package (20, 21). To analyze the heterogeneity of the particles, the images were subjected to Kohonen's self-organizing feature maps (22). After this classification, homogeneous populations were obtained and averaged.

To generate an initial model, either for the nucleotide-free or the ATP-bound samples, selected particles were subjected to a common lines procedure implemented in the EMAN software package (23) imposing C7 symmetry. Working with a total of 11,011 and 8,303 images (for nucleotide-free and ATP-bound samples, respectively) these initial rough models were refined imposing 7-fold or no symmetry using EMAN (23) and SPIDER software subsequently (24). After reaching the convergence of these refinements, the reconstructions yielded resolutions of 23 Å and 24 Å for nonsymmetrized nucleotide-free and ATP-bound structures and of 27 Å for the nonsymmetrized native structure (Fourier Shell Correlation of 0.3 criterion). These models obtained from the negatively stained preparations were scaled and input to a two-independent refinement using 10,312 Cryo-EM particles with or without imposing C7 symmetry, using SPIDER software (24). The resolutions of the final maps were estimated to 12 Å and 18 Å for the nonsymmetrized and symmetrized structures. These values were used to low pass filter the volume in the final model (see Fig. 3*A* and supplemental Fig. S2).

Docking experiments were carried out using SITUS software (25). Volume handling was carried out using XMIPP software (20), and general visualization was performed using Chimera (26) and PyMol (27).

RESULTS AND DISCUSSION

Coexpression of GroEL-GroES and AGXT-LTM Increases the Solubility of the Mutant Protein and Results in the Formation of a GroEL·AGXT-LTM Stable Complex—We first measured the AGXT activity from the soluble extracts when AGXT-LTM was expressed in *E. coli* either in the absence or presence of

GroEL-GroES. Our data show that the AGXT activity of *E. coli* lysates increases when mutant AGXT-LTM is expressed in presence of the GroEL-GroES system (Fig. 1*A*). Western blot analysis shows that this increase in activity is related to the amount of soluble AGXT-LTM mutant protein (Fig. 1*B*). This result indicates that GroEL-GroES coexpression improves, *in vivo*, the yield of soluble and active AGXT-LTM mutant protein.

Lysates overexpressing His-tagged AGXT-LTM and GroEL-GroES were subjected to nickel-affinity chromatography. SDS-PAGE of the eluted fractions showed two bands corresponding to the molecular weight of AGXT-LTM protein and to GroEL protomers. A final purification step by gel filtration chromatography revealed that the largest proportion of AGXT-LTM copurifies as a complex with GroEL (Fig. 1*C*). This result suggests that GroEL captures partially folded copies of AGXT-LTM mutant protein for a folding reaction cycle. Once the cell lysis occurs and the ATP is consumed, the folding reaction is blocked, trapping a stable GroEL·AGXT-LTM complex. The overexpression of the wild-type AGXT together with the GroEL-GroES system produced similar complexes, but the amount of stable and folded AGXT protein predominates (Fig. 1*C*).

The purified complex was then incubated in the presence of a 10 molar excess ATP (ATP-bound) for comparison purposes. The new sample was subjected to the same purification steps, and the analysis of the SDS-PAGE confirms that the GroEL·AGXT-LTM complex is largely maintained in presence of ATP.

Electron Microscopy (EM) Confirms Two Conformational Steps of GroEL Trapping AGXT-LTM mutant—The resulting GroEL·AGXT-LTM complex was stained for observation in the electron microscope to elucidate the nature of the interaction between both proteins before and after the conformational change undergone by GroEL upon ATP binding (see "Experimental Procedures " and supplemental Fig. S1). 11,011 and 8,303 particles of the nucleotide-free and ATP-bound GroEL·AGXT-LTM complex were selected, respectively, and two-dimensional averages were generated using a maximum likelihood two-dimensional reference-free alignment process (Fig. 2*A*). The analysis revealed several classes that encompass the two typical views of GroEL, the end-on view revealing its heptameric nature, and the side view showing its two ring structure. The analysis of these classes confirms the formation of GroEL·AGXT-LTM complexes as the end-on view averages clearly show some extra density at the central folding cavity. The comparison of the equivalent two-dimensional classes corresponding to the nucleotide-free and ATP-bound samples revealed structural changes (supplemental Fig. S1). We analyzed these differences by comparing their low resolution three-dimensional structures generated after angular refinement. 7-fold symmetrized volumes of the two samples were first generated. The comparison of the two three-dimensional reconstructions showed differences both in the conformation of the GroEL chaperonin and in the relative position of the substrate with respect to the chaperonin (Fig. 2, *B* and *C*). The nucleotide-free structure showed approximately a 10% increase in height and width of the GroEL barrel with respect to

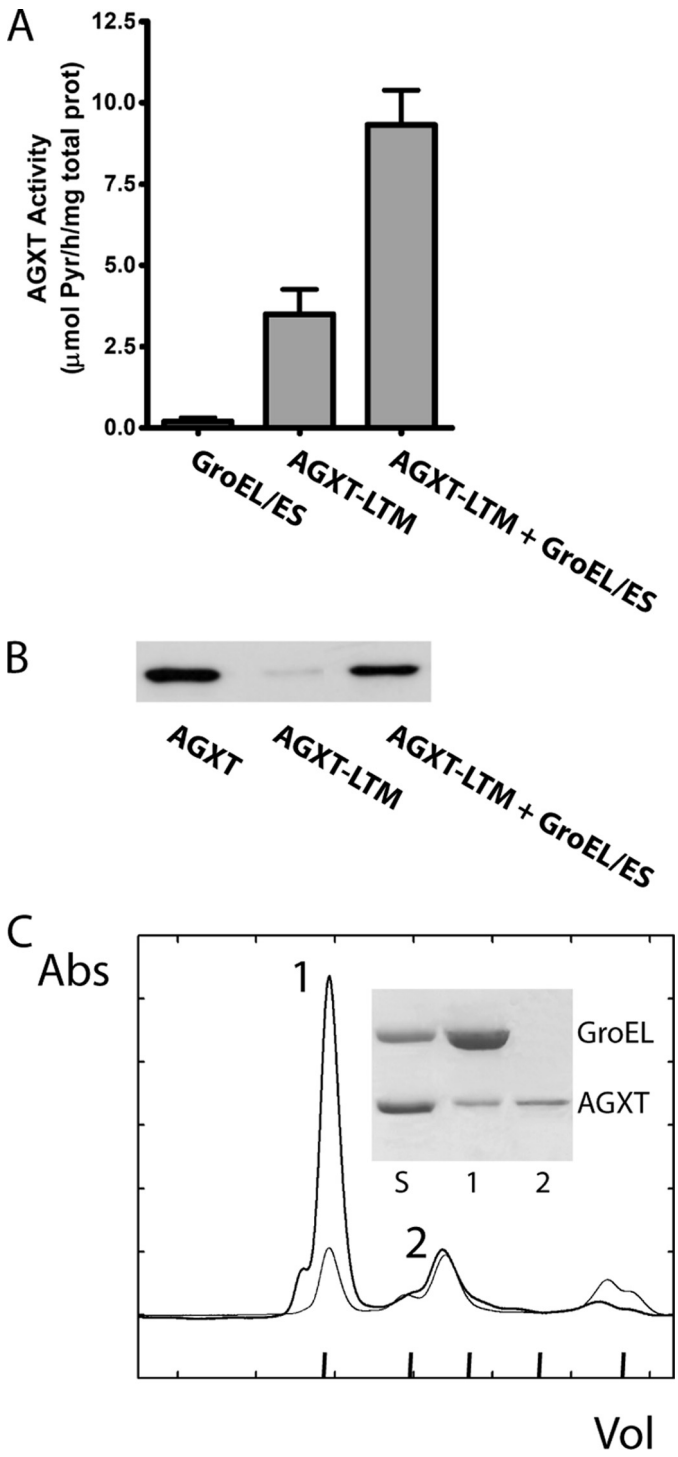

FIGURE 1. **GroEL-GroES system facilitates the folding of AGXT-LTM.** *A*, comparison of the AGXT activity assays performed on cell lysates when expressing either GroEL-GroES alone, AGXT-LTM mutant protein alone, or both GroEL-GroES and AGXT-LTM. The mean values are indicated, and the S.D. values are represented as *error bars*. Calculations have been performed using 10, 14, and 26 independent observations, respectively. *B*, AGXT-LTM protein present in 1 μg of the soluble fraction from *E. coli* pellets with or without coexpression of GroEL-GroES. Soluble wild-type AGXT was included as a control. AGXT was detected by Western blotting with anti-AGXT antibody (1:5,000). *C*, purification of GroEL·AGXT-LTM and GroEL·AGXT (*thick* and *fine lines*, respectively). The elution profile of the gel filtration chromatography and the SDS-PAGE of the sample loaded (*S*) and from each of the two peaks (labeled accordingly) are shown. The column was calibrated using gel filtration standards from Bio-Rad.

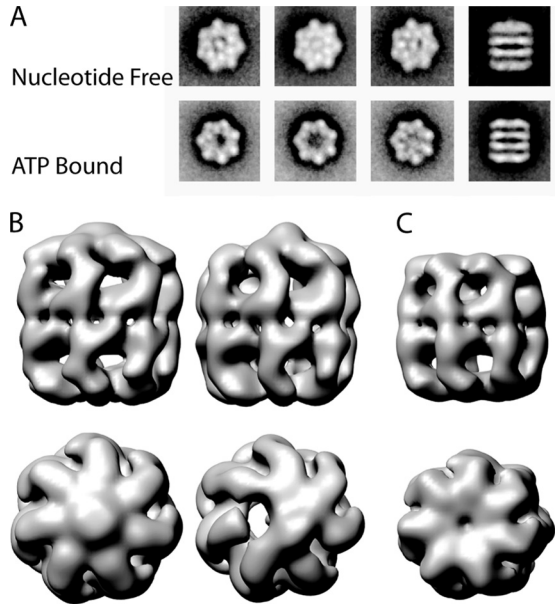

FIGURE 2. **Electron microscopy of GroEL·AGXT-LTM complexes.** *A*, representative subset of two-dimensional average images from a maximum likelihood reference-free alignment of negatively stained native (*upper*) and ATP-bound (*lower*) complexes. *B* and *C*, end-on and side views of the three-dimensional structure of the GroEL complexes: 7-fold symmetrized and non-symmetrized reconstructions of the nucleotide-free sample (*B*) and 7-fold symmetrized reconstruction of the ATP-bound sample (*C*).

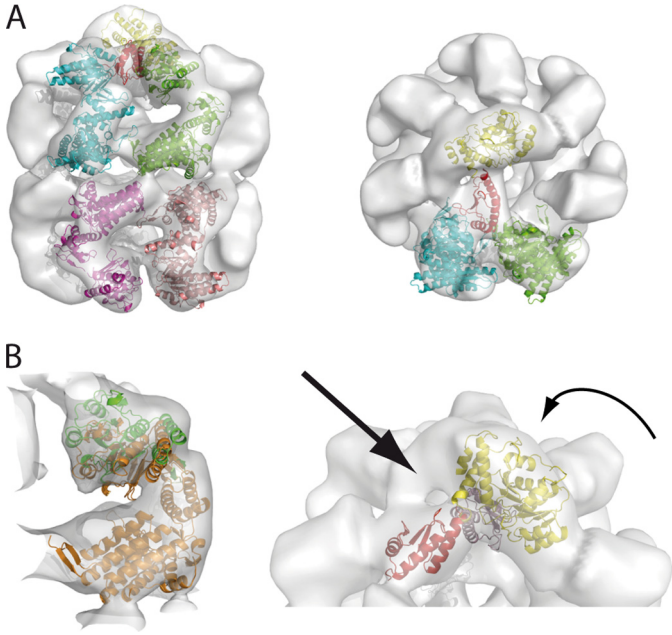

FIGURE 3. *A*, two views of the Cryo-EM three-dimensional structure of the GroEL·AGXT-LTM complex. Docking of the atomic model of GroEL and AGXT onto the three-dimensional reconstruction of the complex is shown. The atomic models corresponding to the N-terminal and C-terminal domains of AGXT are depicted as *yellow* and *red ribbons*, respectively. Some of the GroEL protomers are omitted for clarity of the figure. *B*, details of the fitting of GroEL and AGXT crystal structures into the Cryo-EM map. *Left*, superposition of the fitting of a single GroEL subunit (*orange*) and the conformational changes required to adapt the GroEL apical domain of the subunit into the experimental Cryo-EM map (*green*). *Right*, docking of the N-terminal (*yellow*) and C-terminal (*red*) domains of AGXT and the conformational changes required adapting the C-terminal domain for the original structure (*purple*). The *straight arrow* indicates a region of the AGXT mass that could be filled by the 22 residues of the N-terminal sequence of AGXT omitted from the AGXT atomic model. The *curved arrow* indicates the region of AGXT facing the GroEL folding cavity that is involved in the AGXT dimer formation.

the size of the ATP-bound sample, the latter being similar to the size observed for the substrate-free, nucleotide-free GroEL (10). This enlargement results in an expansion of the folding cavity that has been already reported for other substrate-bound GroEL complexes (28, 29) and has been attributed to the plasticity of the GroEL ring to accommodate large protein substrates. Both complexes display extra density occluding the GroEL cavity that can be uniquely attributed to the presence of the protein substrate. However, this density protrudes from the chaperonin in the nucleotide-free complex and is internalized upon ATP binding.

To characterize further the interactions between GroEL and the bound, unfolded protein, a three-dimensional reconstruction of the two different complexes was attempted without imposing any symmetry. It was not possible to obtain a stable asymmetric model for the ATP-bound preparation. This could be a reflection of heterogeneity in our data set due to substrate structural conformational variability. Indeed, the substrate density in the ATP-bound symmetrical model is considerably smaller than that observed in the nucleotide-free complex. This effect cannot be attributed solely to the application of 7-fold symmetry but also to the variable conformation distribution of the substrate in the GroEL cavity in the ATP-bound complex. Further evidence of this heterogeneity can be found in the analysis of the representative averaged end-on views obtained in the two-dimensional analysis of the samples. Although the nucleotide-free sample appears to be quite homogeneous, the ATP-bound sample is clearly heterogeneous, with the substrate adopting several conformations (see Fig. 2*A*). This is in agreement with the data presented by Elad *et al.* (30) in which unfolded malate dehydrogenase internalized into GroEL cavity adopts several conformations. However, analysis of the low resolution nucleotide-free structure provides information of the nature of the GroEL·AGXT-LTM interaction. The level of resolution of this complex (23 Å) allows the identification of the density corresponding the AGXT-LTM mutant protein. It crosses the GroEL central cavity and makes contact with distant GroEL apical domains.

Cryo-EM Confirms That AGXT-LTM Is Partially Folded and Provides the Visualization of an Early Step of the Folding Reaction Cycle—To define a higher resolution description of the native complex, the sample was subjected to Cryo-EM techniques (see "Experimental Procedures " and supplemental Fig. S2). More than 10,000 particles were selected and prepared for angular refinement methods. The models from the negative stained samples were the input for further refinement. Two independent refinement processes were carried out, with and without imposing 7-fold symmetry. The three-dimensional reconstruction obtained without imposing symmetry allowed us to obtain a model that contains details on the interaction between GroEL and AGXT-LTM mutant, but the resolution obtained was significantly lower. On the contrary, the refinement imposing 7-fold symmetry lacked this detailed information but could achieve better resolution for the chaperone moiety (supplemental Fig. S2). Thus, the final structure shown in Fig. 3*A* represents a composite map formed by the GroEL moiety derived from the structure refined with symmetry and the

substrate mass derived from the volume refined without symmetry. Therefore, the resolution for either section of the model is different: 12 Å for the chaperone and 18 Å for the substrate complex.

The atomic coordinates of the GroEL crystal structure (Protein Data Bank code 1OEL) (31) were fitted into the electron micrograph density map as described under "Experimental Procedures." Considering each GroEL protomer as a rigid body, the analysis of the fitting clearly showed that GroEL apical domains lay outside the map. Then, we proceeded to readjust the position of the domain individually. This rendered an expanded GroEL "open" barrel in which the connections between the two ring structures are maintained but the apical domains are twisted by ~20 degrees (Fig. 3*B*). We did not attempt to carry out any finer adjustments of the atomic coordinates to the Cryo-EM map.

The extra density located in the cavity can be unequivocally assigned to AGXT-LTM, and it is structured in two domains. These are clearly asymmetric, each one interacting with the apical domains of opposite GroEL subunits. AGXT is a homodimer formed by two 43-kDa subunits, whose atomic structure is known (Protein Data Bank code 1H0C)) (16). Each protomer is folded into a large N-terminal domain (residues 22–282) and a smaller C-terminal domain (283–392). Besides, a long unstructured N-terminal tail (residues 1–21) grabs the subunits within the dimer (supplemental Fig. S3). The analysis of the size and shape of the AGXT-LTM density suggests that the protein adopts an almost folded but open conformation in which the two domains of AGXT interact with distant apical domains of GroEL. The AGXT atomic coordinates were used to define its two topological domains and fit into the Cryo-EM density map. Each domain fits well in the Cryo-EM map. Remarkably, the best solutions leave the C terminus of the N-terminal domain and the N terminus of the C-terminal domain in close vicinity, thus being compatible with an AGXT structure displaying an open expanded conformation (Fig. 3*B*). There is an extra density on the top of the oligomer that cannot be resolved in terms of the crystal structure of AGXT, but that could account for residues 1–22 of the AGXT structure. Because of the resolution of our model it is not possible to determine precisely the AGXT regions involved in GroEL binding. Remarkably, the unfolded AGXT interacts solely with the apical domains of GroEL. In this model, the surface patches responsible of the AGXT dimerization face either the hydrophobic patches of the apical domains or the folding cavity of the chaperone. This situation displays a striking similarity to that observed for the chaperonin-containing TCP1 interaction with actin and tubulin (32, 33) in which chaperonin-containing TCP1 stabilizes both cytoskeletal proteins in open and quasi-folded conformations through interactions between distant subunits of the chaperonin ring.

The combined biochemical and structural analysis on the GroEL·AGXT-LTM complexes indicates that we have been able to trap a functional folding intermediate of AGXT-LTM mutant protein that will proceed to its final native structure with the assistance of GroEL. Binding of unfolded AGXT to GroEL involves distant sides of the chaperonin folding cavity so that the substrate displays an expanded conformation. Single-molecule fluorescence resonance energy transfer experiments have demonstrated that subsequent ATP-induced domain movements in GroEL cause the stretching of the substrate and further unfolding and compaction of the substrate on the GroEL surface (13, 14, 15). Indeed, our structural data support this model because we observed that the incubation of the purified GroEL·AGXT-LTM complex with ATP induces the internalization of the density corresponding the AGXT-LTM substrate. Our data also support the model for a chaperone folding reaction cycle in which binding of a quasi-native AGXT to GroEL proceeds in an ATP-independent manner. This conformation could be reached with or without the help of other cofactors, or it could result from an unsuccessful GroEL folding reaction cycle.

Nowadays, the most effective treatment for PH1 consists of either kidney and liver double transplantation or preemptive liver transplantation. Among the new pharmacological therapies under study, the use of chemical chaperones to bind and stabilize a native AGXT protein conformation is very attractive. With early intervention, such a chemoprophylactic approach would minimize renal damage and potentially avoid the significant morbi-mortality of liver transplantation and the adverse effects of immunosuppression. The effectiveness of the treatment would depend on the effect of the pathogenic mutations and subsequent protein conformation changes. Our data show that the aggregation-prone AGXT-LTM mutant protein retains partial function that is also able to form folding intermediates and that the GroEL-GroES system improves the yield of active and soluble protein. Consequently, it represents a promising target for pharmacological chaperones.

REFERENCES

1. Bukau, B., and Horwich, A. L. (1998) *Cell* **92,** 351–366
2. Carrell, R. W., and Lomas, D. A. (1997) *Lancet* **350,** 134–138
3. Caughey, B., and Baron, G. S. (2006) *Nature* **443,** 803–810
4. Broadley, S. A., and Hartl, F. U. (2009) *FEBS Lett.* **583,** 2647–2653
5. Hoppe, B., Beck, B. B., and Milliner, D. S. (2009) *Kidney Int.* **75,** 1264–1271
6. Santana, A., Salido, E., Torres, A., and Shapiro, L. J. (2003) *Proc. Natl. Acad. Sci. U.S.A.* **100,** 7277–7282
7. Williams, E. L., Acquaviva, C., Amoroso, A., Chevalier, F., Coulter-Mackie, M., Monico, C. G., Giachino, D., Owen, T., Robbiano, A., Salido, E., Waterham, H., and Rumsby, G. (2009) *Hum. Mutat.* **30,** 910–917
8. Saibil, H. R., and Ranson, N. A. (2002) *Trends Biochem. Sci.* **27,** 627–632
9. Fenton, W. A., and Horwich A. L. (2003) *Q. Rev. Biophys.* **36,** 229–256
10. Braig, K., Adams, P. D., and Brünger, A. T. (1995) *Nat. Struct. Biol.* **2,** 1083–1094
11. Xu, Z., Horwich, A. L., and Sigler, P. B. (1997) *Nature* **388,** 741–750
12. Hartl, F. U., and Hayer-Hartl, M. (2009) *Nat. Struct. Mol. Biol.* **16,** 574–581
13. Lin, Z., Madan, D., and Rye, H. S. (2008) *Nat. Struct. Mol. Biol.* **15,** 303–311
14. Madan, D., Lin, Z., and Rye, H. S. (2008) *J. Biol. Chem.* **283,** 32003–32013
15. Sharma, S., Chakraborty, K., Müller, B. K., Astola, N., Tang, Y. C., Lamb, D. C., Hayer-Hartl, M., and Hartl, F. U. (2008) *Cell* **133,** 142–153
16. Zhang, X., Roe, S. M., Hou, Y., Bartlam, M., Rao, Z., Pearl, L. H., and Danpure, C. J. (2003) *J. Mol. Biol.* **331,** 643–652
17. Sambrook, J., and Russell, D. W. (2001) *Molecular Cloning: A Laboratory Manual*, 3rd Ed., pp. A8.52–A8.55, Cold Spring Harbor Laboratory Press, Plainview, NY
18. Mindell, J. A., and Grigorieff, N. (2003) *J. Struct. Biol.* **142,** 334–347
19. Heymann, J. B., and Belnap, D. M. (2007) *J. Struct. Biol.* **157,** 3–18
20. Sorzano, C. O., Marabini, R., Velázquez-Muriel, J., Bilbao-Castro, J. R., Scheres, S. H., Carazo, J. M., and Pascual-Montano, A. (2004) *J. Struct. Biol.* **148,** 194–204

21. Scheres, S. H., Núñez-Ramírez, R., Sorzano, C. O., Carazo, J. M., and Marabini, R. (2008) *Nat. Protoc.* **3,** 977–990
22. Marabini, R., and Carazo, J. M. (1994) *Biophys. J.* **66,** 1804–1814
23. Ludtke, S. J., Baldwin, P. R., and Chiu, W. (1999) *J. Struct. Biol.* **128,** 82–97
24. Frank, J., Radermacher, M., Penczek, P., Zhu, J., Li, Y., Ladjadj, M., and Leith, A. (1996) *J. Struct. Biol.* **116,** 190–199
25. Chacón, P., and Wriggers, W. (2002) *J. Mol. Biol.* **317,** 375–384
26. Pettersen, E. F., Goddard, T. D., Huang, C. C., Couch, G. S., Greenblatt, D. M., Meng, E. C., and Ferrin, T. E. (2004) *J. Comput. Chem.* **25,** 1605–1612
27. DeLano, W. L. (2002) *The PyMOL Molecular Graphics System*, DeLano Scientific LLC, San Carlos, CA
28. Clare, D. K., Bakkes, P. J., van Heerikhuizen, H., van der Vies, S. M., and Saibil, H. R. (2009) *Nature* **457,** 107–110
29. Chen, D. H., Song, J. L., Chuang, D. T., Chiu, W., and Ludtke, S. J. (2006) *Structure* **14,** 1711–1722
30. Elad, N., Clare, D. K., Saibil, H. R., and Orlova, E. V. (2008) *J. Struct. Biol.* **162,** 108–120
31. Braig, K., Otwinowski, Z., Hegde, R., Boisvert, D. C., Joachimiak, A., Horwich, A. L., and Sigler, P. B. (1994) *Nature* **371,** 578–586
32. Llorca, O., McCormack, E. A., Hynes, G., Grantham, J., Cordell, J., Carrascosa, J. L., Willison, K. R., Fernandez, J. J., and Valpuesta, J. M. (1999) *Nature* **402,** 693–696
33. Llorca, O., Martín-Benito, J., Grantham, J., Ritco-Vonsovici, M., Willison, K. R., Carrascosa, J. L., and Valpuesta, J. M. (2001) *EMBO J.* **20,** 4065–4075